

This work was written as part of one of the author's official duties as an Employee of the United States Government and is therefore a work of the United States Government. In accordance with 17 U.S.C. 105, no copyright protection is available for such works under U.S. Law.

Public Domain Mark 1.0

<https://creativecommons.org/publicdomain/mark/1.0/>

Access to this work was provided by the University of Maryland, Baltimore County (UMBC) ScholarWorks@UMBC digital repository on the Maryland Shared Open Access (MD-SOAR) platform.

Please provide feedback

Please support the ScholarWorks@UMBC repository by emailing scholarworks-group@umbc.edu and telling us what having access to this work means to you and why it's important to you. Thank you.

Numerical simulation of Alfvénic turbulence in the solar wind

M. L. Goldstein,¹ D. A. Roberts,¹ A. E. Deane,² S. Ghosh,^{1,3}
and H. K. Wong^{1,4}

Abstract. Low-frequency fluctuations in the solar wind magnetic field and plasma velocity are often highly correlated, so much so that the fluctuations can be thought of as nearly perfect Alfvén waves. Evidence from the Helios and Ulysses spacecraft suggest strongly that these fluctuations emanate from the solar corona with high correlation and flat power spectra ($\sim f^{-1}$). These fluctuations constitute a source of free energy for a turbulent cascade of magnetic and kinetic energy to high wave numbers, a cascade that evolves most rapidly in the vicinity of velocity shears and the heliospheric current sheet. Numerical solutions of both the compressible and incompressible equations of magnetohydrodynamics (MHD) in Cartesian geometry showed that sharp gradients in velocity would decrease substantially the Alfvénicity of initially pure Alfvénic fluctuations; however, the effects of solar wind expansion on this turbulent evolution is, as yet, undetermined. We demonstrate that as was the case in Cartesian geometry, in an expanding volume, velocity shears and pressure-balanced flux tubes still reduce the Alfvénicity of parallel propagating wave packets. These three-dimensional spherically expanding simulations include velocity shears separating fast and slow flows, pressure-balanced flux tubes, and a central current sheet which is the site of magnetic reconnection. Two-dimensional spectra constructed in the $r - \theta$ plane resemble closely those resulting from similar initial conditions in Cartesian geometry.

1. Introduction

The earliest descriptions of the solar wind plasma suggested that it displayed many attributes of a turbulent magnetofluid. *Coleman* [1968] noted that the power spectra of magnetic field fluctuations resembled closely those found in hydrodynamic turbulence in that they had power law indices close to the Kolmogoroff value of $5/3$. How this turbulence might be generated was not, however, obvious, in part because the solar wind contains nearly pure Alfvén waves [*Belcher and Davis*, 1971; *Coleman*, 1967], which are exact solutions of the dissipationless and incompressible magnetohydrodynamic (MHD) equations. Thus, to the extent that the solar wind is both incompressible and dissipationless, the presence of Alfvén waves should inhibit the development of turbulence. *Coleman* noted, however, that there was sufficient energy in the interactions between fast and slow solar wind streams to drive a turbu-

lent cascade, although the mechanism for accomplishing this was unclear. The most obvious candidate, the Kelvin-Helmholtz instability, is suppressed by the average Archimedean spiral magnetic field [*Parker*, 1964].

In a series of studies, *Bruno et al.* [1985], *Roberts et al.* [1987a,b], and *Bavassano et al.* [1998] have shown that the Alfvénic nature of the magnetic field and velocity fluctuations decreases with increasing heliocentric distance. The decrease is correlated with proximity to regions of strong velocity shear. One of the goals of theoretical studies of the solar wind has been to understand the mechanisms which drive the evolution of Alfvén waves in the solar wind. In the next section, we summarize briefly the observational background that motivates this research. In section 3, we describe past work modeling the generation of turbulent cascades in rectangular geometry. Much of that work used spectral methods to solve the MHD equations. In section 4, we discuss some recent work modeling the generation of Alfvénic turbulence in spherical geometry. The paper concludes with a discussion of the implications of the current work.

2. Observational Background

The Alfvénic nature of the solar wind is remarkable; almost any randomly selected interval of magnetic field and plasma data is characterized by highly

¹NASA Goddard Space Flight Center, Greenbelt, Maryland.

²Institute for Physical Science and Technology, University of Maryland, College Park.

³Also at SM&A Corporation, Largo, Maryland.

⁴Also at Universities Space Research Association, NASA Goddard Space Flight Center, Greenbelt, Maryland.

aligned fluctuations. Alfvénic intervals tend to be associated with high speed streams, although many examples of Alfvénic flows can be found in slow wind. In this paper, we ignore pressure anisotropies in the solar wind plasma, and define Alfvén waves to be fluctuations which satisfy $\delta\mathbf{v} = \pm\delta\mathbf{b}$, where $\delta\mathbf{v}$ and $\delta\mathbf{b}$ are the fluctuating velocity and magnetic fields, respectively, and $\delta\mathbf{b}$ is normalized to Alfvén speed units, that is, $\delta\mathbf{b} = \delta\mathbf{B}/\sqrt{4\pi\rho_0}$, where ρ_0 is the average plasma density and \mathbf{B} is the magnetic field in cgs units.

The degree of Alfvénicity of solar wind fluctuations can be measured by the cross helicity defined by $H_c = \frac{1}{2} \int d\mathbf{x}^3 \delta\mathbf{v} \cdot \delta\mathbf{b}$. More useful than the global cross helicity, is the normalized quantity $\sigma_c(k)$, which we refer to as the “reduced” normalized cross helicity, defined by $\sigma_c(k) \equiv 2H_c^r(k)/E^r(k)$. The term reduced refers to integrating the spectral tensor over the two directions transverse to the direction of the solar wind velocity so that the spectra are only functions of wave number \mathbf{k} parallel to \mathbf{V}_{SW} . $E^r(k)$ is the reduced spectral energy. Often, however, direct time domain correlations are used to find detailed correlations between solar wind structures, such as velocity shears, and Alfvén wave properties (see, for example, *Roberts et al.* [1987b] and the review by *Goldstein et al.* [1997]).

As proof of the existence of solar wind Alfvén waves, one usually is referred to the seminal work by *Belcher and Davis* [1971], or plots of σ_c , as referenced above. It is illustrative, however, to see just how extraordinarily well correlated fluctuations in the solar wind magnetic and velocity fields are in other regions of the heliosphere. Figure 1 shows a plot of randomly selected data from Ulysses. These data were obtained toward the end of 1994 as Ulysses left the region of the heliospheric current sheet and entered the fast polar wind. The data consist of 8-min averages of vector measurements of the magnetic field (normalized to Alfvén speed units) and vector measurements of velocity fluctuations. A high degree of correlation is evident during this time interval.

Studies using data from Helios 1 and 2 and Voyager 1 and 2 showed that the regions of strong velocity shear which accompany recurrent high speed streams are characterized by rapid decreases in σ_c (see *Bavassano and Bruno* [1989] and *Bavassano et al.* [1998]). Dynamical evolution of solar wind turbulence is evidenced by the fact that σ_c decreases with increasing radial distance from values very close to unity at 0.3 AU. Other studies have shown convincing evidence that compressive effects also contribute to the decrease in σ_c [*Bruno and Bavassano*, 1991].

A fascinating puzzle of research on solar wind turbulence is that we have very little idea of its symmetry properties. We have known since *Belcher and Davis* [1971] that the variances of solar wind fluctuations are not isotropic. Determining the spectral symmetry properties of the fluctuations requires specifying the three-dimensional wave vector dependence of either

the magnetic or velocity power spectral tensor. From single spacecraft data this is very difficult to do and remains a challenge for future multipoint missions. The common occurrence of Alfvén waves in the solar wind suggests that a reasonable model of the spectral tensor might be the “slab” model, in which all nonzero spectral amplitudes are associated with \mathbf{k} parallel to the ambient magnetic field. Another possibility is the isotropic model, in which wave vectors with the same magnitude all have equal spectral amplitudes. A model which has excited considerable interest and research in the past few years is quasi-two-dimensional, in which wave vectors are nearly perpendicular to the large-scale magnetic field \mathbf{B} , while the magnetic fluctuations are orthogonal to both \mathbf{k} and the local mean magnetic field \mathbf{B}_0 .

It is difficult to find evidence of spectral anisotropies in the solar wind using data from a single spacecraft, although early work suggested that such anisotropies were present [*Sari and Valley*, 1976]. *Matthaeus et al.* [1990], using long stationary data intervals, constructed an ensemble from which they were able to estimate the two-dimensional correlation function. Their results suggested that the ensemble of data was neither “slab-like” Alfvén waves nor isotropic. Rather, the correlation function consisted of two populations: fluctuations with large correlation lengths transverse to \mathbf{B}_0 (Alfvénic) and fluctuations with large correlation lengths parallel to \mathbf{B}_0 (quasi-two-dimensional). Other work has examined the possibility that the non-Alfvénic component of the fluctuations involves “structures” with magnetic fluctuations parallel to \mathbf{B}_0 [see *Ghosh et al.*, 1998b; *Carbone et al.*, 1995 and references therein].

A significant quasi-two-dimensional component of interplanetary fluctuations would have profound implications for energetic particle transport throughout the heliosphere. In quasi-two-dimensional turbulence, pitch

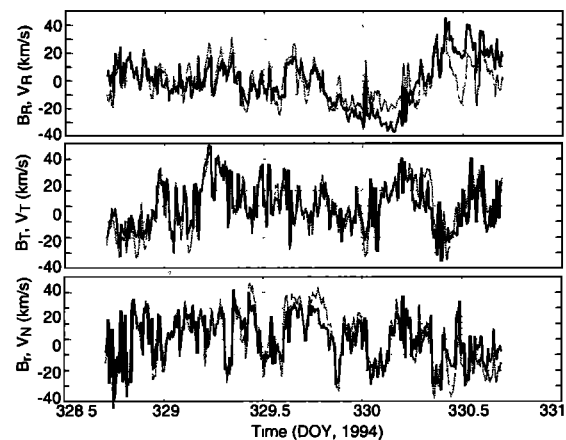


Figure 1. Ulysses data from December 1994. Plotted are the three vector components (in the standard RTN heliospheric coordinate system) of 8-min averages of the fluctuating magnetic field (thin lines) and velocity field (thick lines) illustrating the presence of Alfvén waves.

angle scattering by resonant wave-particle interactions is suppressed [Matthaeus *et al.*, 1990; Bieber *et al.*, 1994]. Furthermore, the direction of minimum variance of magnetic fluctuations is then parallel to \mathbf{B}_0 .

3. Some Previous Simulation Results in Rectangular Geometry

Initial numerical simulations of solar wind turbulence solved the incompressible MHD equations (i.e., $\nabla \cdot \mathbf{v} = 0$) in two spatial dimensions (see discussion by Roberts *et al.* [1991]). These studies suggested that an important factor controlling the evolution of the cross helicity was proximity to both the heliospheric current sheet, where the direction of the radial component of the magnetic field reverses, and regions of strong velocity shear. One limitation of two-dimensional simulations is that the magnetic field must be zero at the center of the current sheet, thus reducing the threshold for velocity shear instabilities. However, that restriction was relaxed by Stribling *et al.* [1996], who used a three-dimensional simulation (also incompressible) and obtained similar results. In the three-dimensional simulation the dc magnetic field rotated through 180° .

More recently, fully compressible codes have been used to simulate solar wind turbulence. Such studies have focused on the role compressibility might play in the evolution of turbulence. Observationally, compressive regions are not highly correlated with a decrease in Alfvénicity [Roberts *et al.*, 1987a; Roberts, 1990]. However, density fluctuations may be significant in other ways [Goldstein *et al.*, 1995]. For example, especially at solar minimum, regions with structured density and other plasma properties show both developed turbulence spectra and strong cross helicity depletions [Bavassano and Bruno, 1989; Grappin *et al.*, 1991; Marsch and Tu., 1989, 1990a,b], but these phenomena are not necessarily due to effects of compressibility.

We know that compressive structures are frequently nearly pressure-balanced [see, e.g., Burlaga and Ogilvie, 1970; Roberts, 1990; Roberts *et al.*, 1987a; Vellante and Lazarus, 1987]. Compressible simulations provide some support for the nearly incompressible model. Roberts *et al.* [1991] ran a two-dimensional compressible MHD simulation with a current sheet, an initial turbulent sonic Mach number of 0.3, and polytropic index of $\gamma = 5/3$. The results were nearly identical (for the evolution of the “incompressible” quantities) to those found using incompressible MHD codes. In both the incompressible and compressible simulations the two-dimensional boxes were initialized with a broadband distribution of Alfvén waves. The simulations indicated that the density fluctuations arose naturally from the incompressible evolution [Matthaeus *et al.*, 1991; Montgomery *et al.*, 1987].

In Figure 2 we show a comparison of Helios data near the heliospheric current sheet together with the results of incompressible and compressible two-dimensional

simulations designed to study and model how the cross helicity is affected by both velocity shear and a current sheet. The results are taken from Roberts *et al.* [1991, 1992]. A similar calculation using a three-dimensional spectral method incompressible calculation can be found in the work of Stribling *et al.* [1996]. These simulations were designed to model the current sheet crossing observed by Helios. In both the experimental and numerical examples, the minimum in the cross helicity occurs in the low-speed region, with the lowest values of σ_c at the current sheet where the radial magnetic field changes sign. For this particular set of simulations, the compressible solutions evolve nearly identically to the “incompressible” solutions. The anticorrelation between $|B|$ and ρ , denoted by $r_{B,\rho}$, suggests that the density fluctuations are nearly pressure-balanced “pseudosound.” The density fluctuations also correlate well with the Elsässer variable, δz^- [cf. Grappin *et al.*, 1990]. (The Elsässer variables [Elsässer, 1950, 1956] are defined by $\mathbf{z}^\pm = \delta \mathbf{v} \pm \delta \mathbf{b}$, where \mathbf{z}^+ and \mathbf{z}^- refer to waves propagating “outward” and “inward” with respect to \mathbf{B}_0 .) Another suggestion concerning the $r_{B,\rho}$ correlation was suggested by Malara *et al.* [1997], who showed that the sign of $r_{B,\rho}$ could be positive in plasmas with $\beta \sim 1$, which is not far from the situation in the solar wind. Positive correlations could also be indicative of the presence of fast mode waves. Positive $r_{B,\rho}$ is observed, especially in slow flows, and such fluctuations may not be in pressure balance as described by nearly incompressible theory. Solar wind fluctuations are, not surprisingly, characterized by several paradigms, depending on the location, flow regime, etc.

4. Inflow Simulations and Spherical Geometry

Although we can learn a surprising amount about the evolution of solar wind turbulence from two- and three-dimensional spectral simulations in Cartesian geometry, there are fundamental problems that these codes cannot address. One limitation has been the use of periodic boundary conditions which assume that following the time evolution is approximately equivalent to following the solar wind in space. While this is perhaps a reasonable approximation when modeling small spatial scales or as a means of investigating the role of velocity shear, it fails for evolution on the scale of an astronomical unit (AU) or more. A related problem is that the spectral simulations do not take into account the spherical expansion of the solar wind, which may be justifiable when studying phenomena with scale sizes smaller than an AU, but the timescale over which such simulations are valid is severely limited.

One approach to modeling the spherical expansion without actually solving the equations in spherical coordinates is that taken by Grappin *et al.* [1993a,b] and Grappin and Velli [1996], who developed a solution technique in which the simulation domain is in comobile

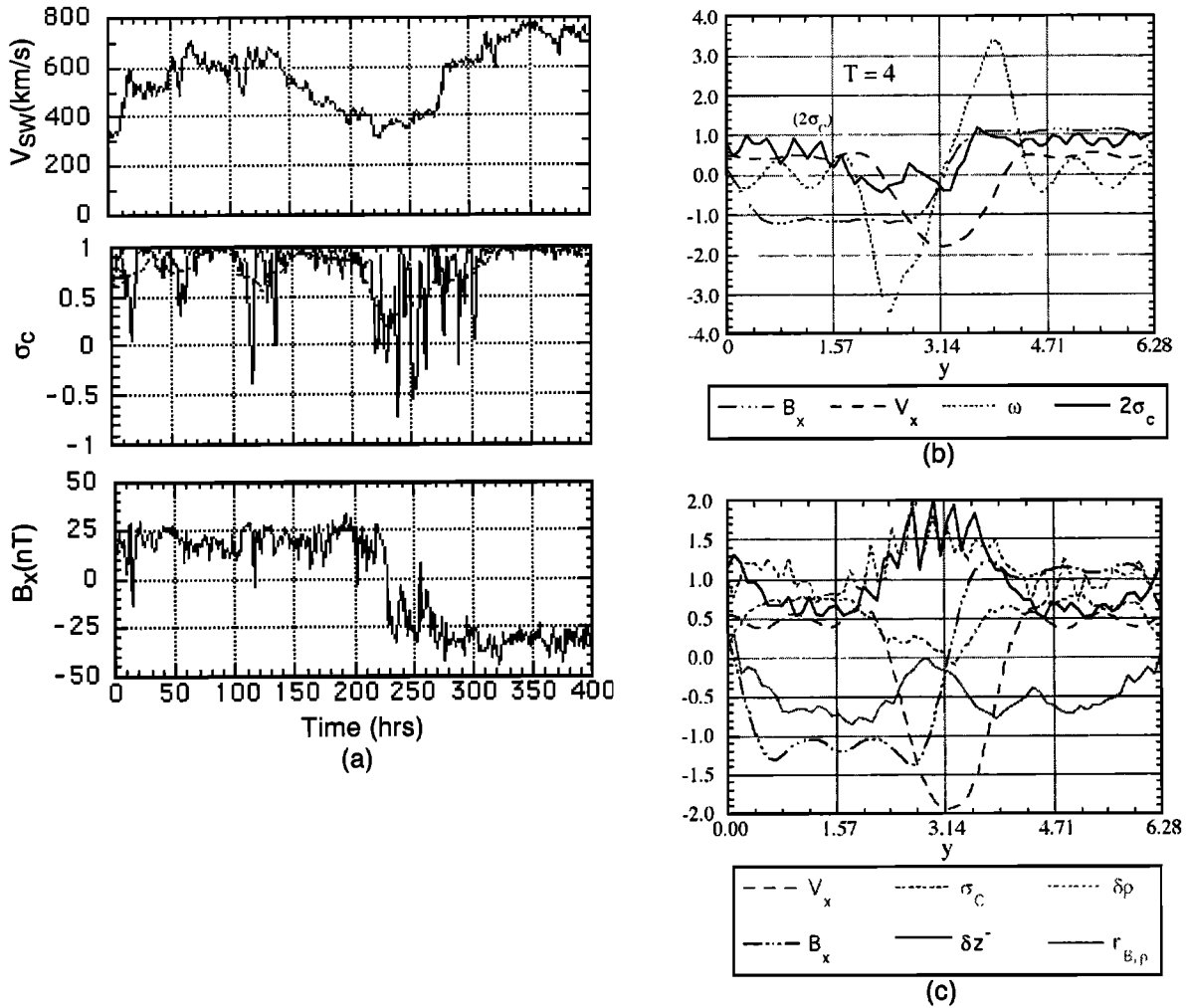


Figure 2. A comparison of Helios data with two-dimensional simulations. (a, left): Hourly averaged Helios 2 data obtained near 0.3 AU (days 93-110 of 1976). Plotted are V_{SW} , σ_c at the scale of about 3 hours (solid line) and a 25-hour running mean (dashed line), together with the radial component (“ B_x ”) of the magnetic field [from *Roberts et al.*, 1992]. (b, top right): Results at $T = 4$ eddy-turnover times from a solution of incompressible MHD, including the vorticity ω [adapted from *Roberts et al.*, 1991]. (c, bottom right): Results at $T = 2$ eddy-turn-over times from a solution of the compressible equations. Similar to (4b), with the addition of density fluctuations, $\delta\rho$; the fluctuating component of “inward propagating” Alfvén waves, δz^- , and the correlation between density and magnetic field magnitude, $r_{B,\rho}$ ($\delta\rho$ and δz^- are normalized to twice their maximum values of 0.042 and 0.075, respectively) [adapted from *Roberts et al.*, 1991].

coordinates, that is, with time the simulation domain expands as though one were moving radially outward in the solar wind. The flow in the radial direction is still periodic, however. On the basis of their calculations, *Grappin et al.* [1993b] and *Grappin and Velli* [1996] have questioned whether or not the expanding solar wind can indeed support a turbulent cascade and suggested that the spherical expansion slows nonlinear interactions to the point that there is essentially no dynamical evolution.

To address issues raised by *Grappin et al.* [1993b] and *Grappin and Velli* [1996] and to employ more realistic boundary conditions, we developed a new simulation code to solve the MHD equations in three dimensions in spherical coordinates. At present, this algorithm

uses inflow (and outflow) supersonic and superAlfvénic boundary conditions in the radial direction and either periodic boundary conditions or various types of outflow boundary conditions in the two orthogonal directions, θ and ϕ . The code can also be run in rectangular coordinates.

4.1. Flux-Corrected Transport

To study the temporal evolution of turbulence in rectangular or spherical geometry we use a fourth-order method based on the flux corrected transport (FCT) algorithm [*Boris and Book*, 1973; *Zalesak*, 1979]. The FCT procedure has been employed previously for MHD by *DeVore* [1991] and S. Zalesak and D. Spicer (private communication, 1996). An important feature of this al-

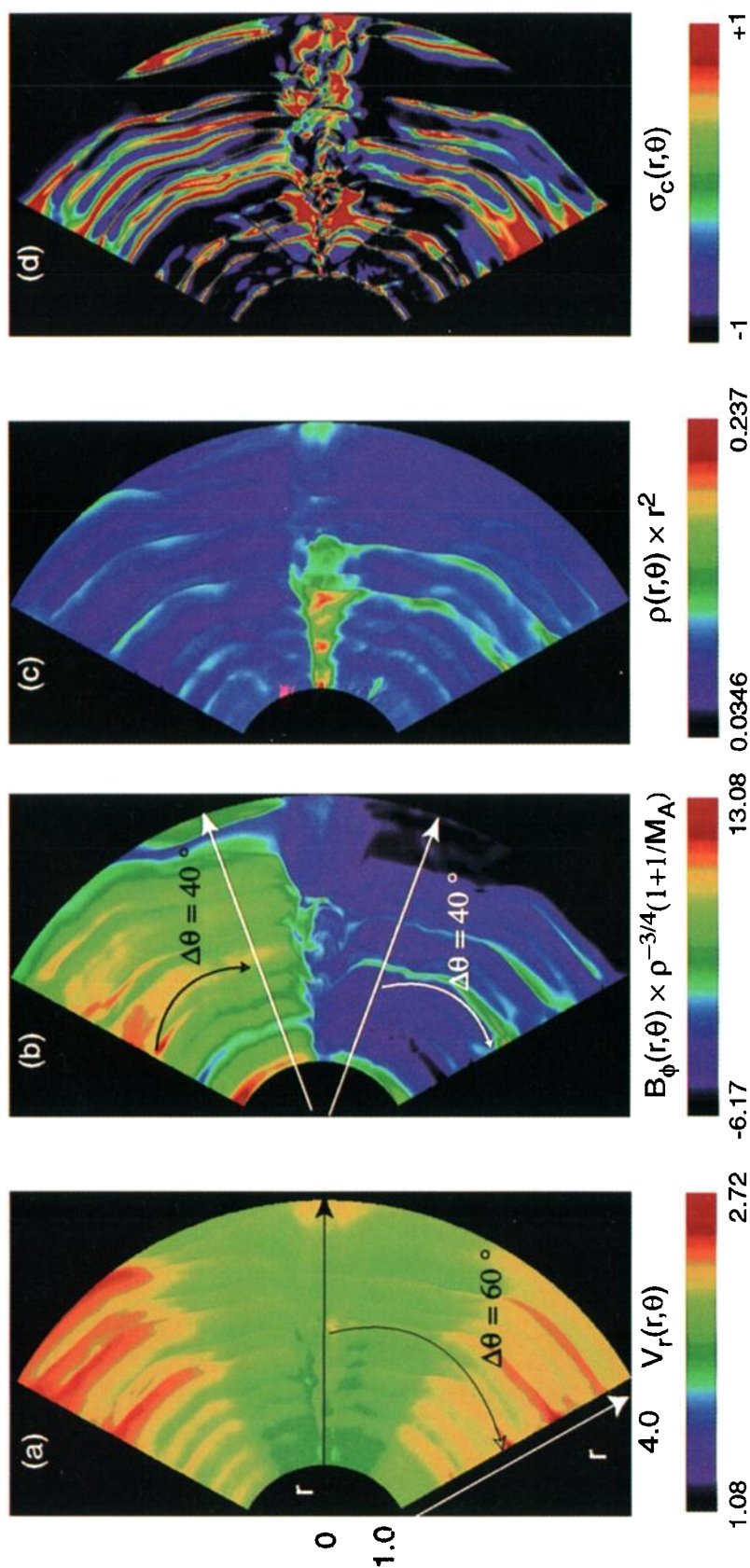


Plate 1. Contours of four quantities from the two-dimensional simulation: (a) $V_r(r, \theta)$, (b) $B_\phi(r, \theta) [\rho^{-3/4}(1 + 1/M_A)]$, (c) $\rho \times r^2$, (d) $\sigma_c(r, \theta)$

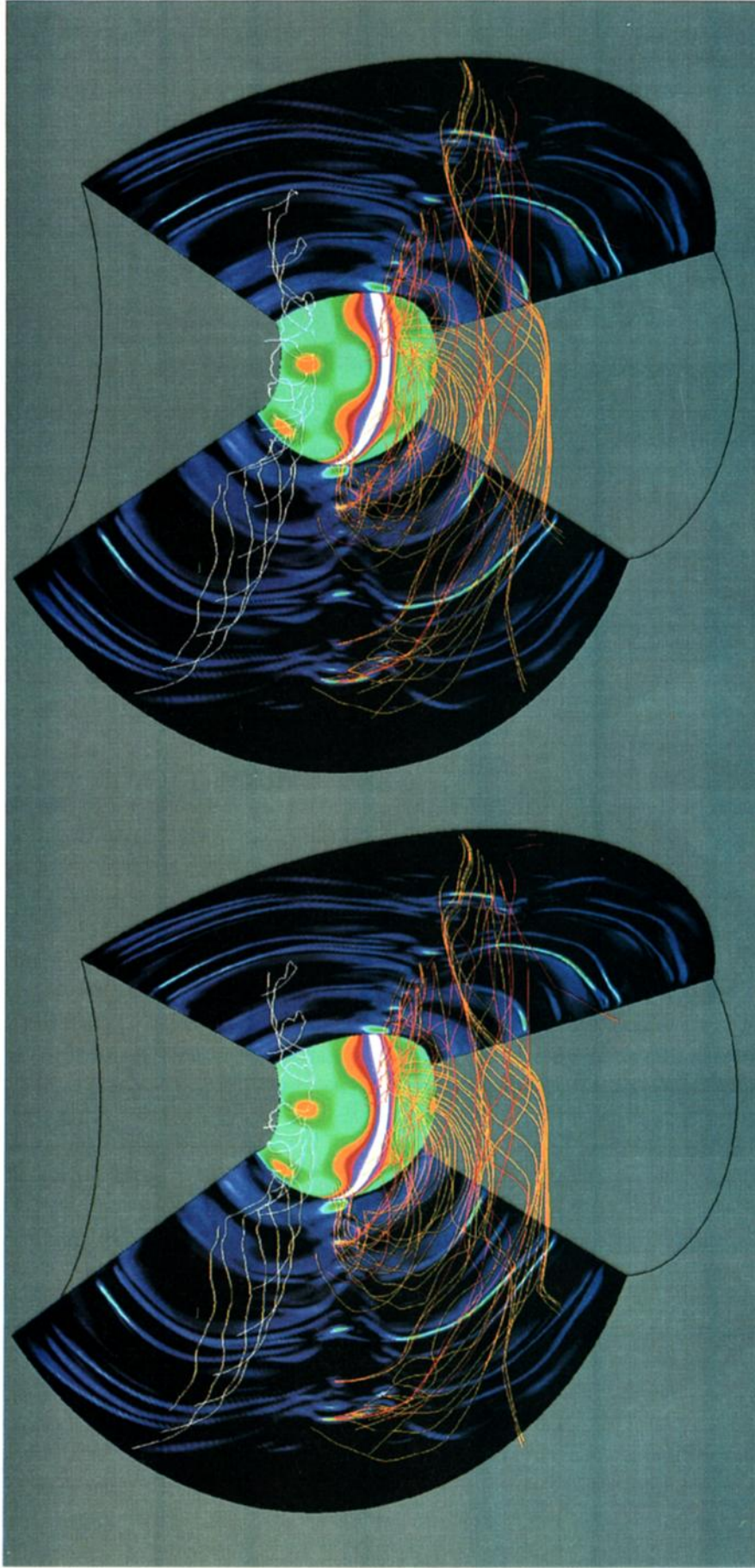


Plate 2. A (“cross-eyed”) (stereo view of the source surface density at $r_0 = 1.0$ and two planes of $j^2 \times r^2$).

gorithm is its capacity to capture shocks and preserve discontinuities. This property is essential if we are to describe the generation and evolution of compressible turbulence characterized by highly nonlinear situations and high Mach numbers. The code solves the inviscid compressible MHD equations in conservation form and is a generalization of a rectangular geometry version described by *Deane* [1996]. The FCT algorithm proceeds by first forming a low-order and a high-order flux. Then an “antidiffusive” flux is constructed as their difference. This is subsequently flux-limited to prevent the formation of spurious extrema. Finally, the solution is updated based on the low-order solution and the antidiffusive flux [*Zalesak*, 1979]. A description of the spherical geometry version of the code can be found in the work of A. Deane et al. (A 3D compressible MHD code in spherical coordinates for solar wind studies, in preparation, 1999).

The magnetic field is calculated from the electric field using Faraday’s law. The cell-averaged magnetic field is cell centered, while the electric field is edge based. This ensures that the code preserves $\nabla \cdot \mathbf{B} = 0$ to within numerical roundoff. The code advances the primary cell-averaged variables of density, the vector momentum, the total energy (internal + kinetic + magnetic), and the vector magnetic field. The equation of state is taken to be that of an ideal gas ($p = \rho RT$).

We turn now to explore the role of velocity shears and current sheets in three-dimensional expanding flows containing Alfvénic wave packets.

4.2. Spherical Geometry

In spherical coordinates, most of the terms can be written in conservation form. Any nonconservative terms are treated as source terms for the otherwise conservative equations. The conservative terms are treated in a straightforward manner by the inclusion of the appropriate metric coefficients in the formation of the various fluxes required by the algorithm. While the source terms are not fluxes in themselves, they do influence the flux limiting.

The MHD equations as solved in the code are

$$\frac{\partial \rho}{\partial t} + \nabla \cdot \rho \mathbf{u} = 0 \quad (1)$$

$$\frac{\partial \rho \mathbf{u}}{\partial t} + \nabla \cdot \left[(p + \frac{B^2}{8\pi}) \mathbf{I} + \rho \mathbf{u} \mathbf{u} - \frac{1}{4\pi} \mathbf{B} \mathbf{B} \right] = 0 \quad (2)$$

$$\frac{\partial}{\partial t} \left(\rho e + \frac{1}{2} \rho u^2 + \frac{B^2}{8\pi} \right) + \nabla \cdot \left[\left(\rho e + \frac{1}{2} \rho u^2 + p \right) \mathbf{u} - \frac{1}{4\pi} (\mathbf{u} \times \mathbf{B}) \times \mathbf{B} \right] = 0 \quad (3)$$

$$\frac{\partial \mathbf{B}}{\partial t} + \nabla \cdot [\mathbf{u} \mathbf{B} - \mathbf{B} \mathbf{u}] = 0 \quad (4)$$

with the relations

$$\nabla \cdot \mathbf{B} = 0 \quad p = (\gamma - 1) \rho e. \quad (5)$$

Equation (5) is consistent with the ideal gas law, $p = \rho RT$. Here \mathbf{I} is the unit tensor with components δ_{ij} and γ is the ratio of specific heats. We write the equations in spherical coordinates, using fluxes where possible and adding source terms in the final step of the integration.

We know from two- and three-dimensional simulations that in rectangular geometry strong gradients in the velocity initiate a turbulent cascade when a broadband spectrum of Alfvén waves is present. In expanding flows the rapid expansion might suppress or slow the generation of turbulence, as conjectured by *Grapin and Velli* [1996]. We first describe the general setup of the simulations and their initial conditions. We then proceed with some simple tests of the algorithm and then construct several velocity shear flow situations and examine their evolution in time and space.

4.3. Initial Conditions

As noted above, single spacecraft measurements in the supersonic and superAlfvénic solar wind have not yielded a three-dimensional picture of the symmetry properties of the fluctuations. That, of course, is not a restriction in a three-dimensional simulation. Nonetheless, it is convenient for comparison with spacecraft data to include in the simulation “virtual spacecraft” that is, probes that collect magnetic field, velocity, and density “data” as one-dimensional time series. We included up to 40 such probes distributed in r , θ , and ϕ . Because the flow was superAlfvénic and supersonic, we were able to use the *Taylor* [1938] frozen-in-flow approximation to construct “reduced” spectra from the probe data.

To include the effects of velocity shear, the simulation domain contained two velocity shear layers in the middle of the volume at $\theta = 1/3$ and $2/3$ of the total wedge angle, which was $\Delta\theta \sim 120^\circ$ for the results discussed in this paper. Slower, denser plasma occupied the middle third of the box as it does in the heliosphere. The velocity was uniform in azimuth, ϕ , and the θ variation was of the form

$$v_r(\theta) = \frac{1}{2} \begin{cases} v_M + v_m + (v_m - v_M) \tanh \frac{\theta - \frac{3\pi - \theta_0}{6}}{\Delta}, & \theta \leq \frac{\pi}{2}, \\ v_M + v_m - (v_m - v_M) \tanh \frac{\theta - \frac{3\pi + \theta_0}{6}}{\Delta}, & \theta > \frac{\pi}{2}. \end{cases} \quad (6)$$

where $v_m < v_M$, and $\Delta \ll \theta_0$, so that $v_0 \approx v_M$ in the upper and lower thirds of the box and $v_0 \approx v_m$ in the slow flow. For the runs described below, $\theta_0 = 120^\circ$, $v_M - v_m = 0.45$, and $\Delta \lesssim 1^\circ$. The mean flow speed $v_0 = (v_M + v_m)/2 = 3$. Therefore the transit time of the waves across the box ($\Delta r = 3$) was 1.

The fluid flow into the volume at $r = r_0 = 1$ was both superAlfvénic and supersonic with Alfvénic and sonic Mach numbers $M_A = 1.5$ and $M = 3.0$, respec-

tively. The flow remained supersonic and superAlfvénic to the outflow boundary at $r = r_{\max} = 4.0$. In the ϕ -direction the flow was taken to be periodic and in both the θ - and r -directions we used linear extrapolation outflow boundary conditions. The radial magnetic field was initially assumed to be independent of θ and to fall-off with r as $B_r(r, \theta, \phi) = B_0(r_0/r)^2$. The radial density profile was defined using an approximation to Parker's asymptotic solution [Parker, 1963]. The initial density at $r = r_0$ was $\rho_0 = 1/4\pi$. Consequently, the average Alfvén speed at the inflow boundary was $V_A = B_0$. For the results discussed below, $B_0 = 1$. The temperature is not a dynamical variable, but it is taken (implicitly) to be uniform on the inflow boundary.

When pressure-balanced structures are present, they are defined as longitudinal field perturbations (with $k_{\parallel} = 0$) such that

$$B_r(\theta, \phi) = \left(\frac{r_0}{r}\right)^2 B_0(r_0) + \left(\frac{r_0}{r}\right)^2 B_1 \cos \left[\left(\frac{2\pi}{\theta_0} \right) (k_{\theta} \theta) \right] \cos \left[\left(\frac{2\pi}{\phi_0} \right) (k_{\phi} \phi) \right] \quad (7)$$

where $\theta_0 = \phi_0 = 120^\circ$, $k_{\theta} = k_{\phi} = 2$, and either $B_1 = 0$ or $B_1 = 0.2$. These structures, when nonzero, are present initially (to preserve $\nabla \cdot \mathbf{B} = 0$) and are applied to the inflow boundary for all subsequent times.

One property of the solar wind sometimes included in these spherically expanding simulations is the Parker spiral magnetic field. This field does not arise naturally in our model because we are not in a rotating coordinate system. However, it is easy to include by adding a constant b_{ϕ} at the inflow boundary and letting it convect into the simulation domain. Because B_r falls off approximately as $1/r^2$, this constant b_{ϕ} becomes increasingly important with increasing r , creating a global spiral pattern. In those runs which included a Parker spiral component to the field, we used $b_{\phi} = 1/4 B_0$.

To model the heliospheric current sheet, we have modified the background radial magnetic field so that it rotates by π radians in the middle of the slow flow region. This is accomplished in part using a tanh function so that $B_r(r, \theta, \phi) = B_0(r) \tanh[(\theta - \pi/2)/\Delta]$ so that the radial field changes sign across the current sheet. To keep the average field from being zero in the central current sheet region, which is both unphysical because the solar wind field is rarely close to zero and problematic because very small values of the field increase dramatically compressive effects that become difficult to integrate, we constructed a rotation of the field through the current sheet by adding in ϕ and r components to remove the zero in $|B|$. The added components are defined by

$$B_{\phi}(r_0, \theta) = -\delta b_{cs} \operatorname{sech} \frac{\theta - \pi/2}{\Delta} \\ B_r(r_0, \theta) = \delta b_{cs} \operatorname{sech} \frac{\theta - \pi/2}{\Delta} \quad (8)$$

where δb_{cs} is a measure of decrease in field magnitude in the middle of the current sheet. In the runs described below, $\delta b_{cs} = 1/3$. B_{ϕ} is independent of the Parker spiral component, b_{ϕ} .

Initially, the volume of integration is empty of fluctuations and the pressure is initialized so that there is pressure balance with the magnetic field. At $t = 0$ a parallel propagating Alfvén wave packet convects and propagates into the volume. In the runs described below, the wave packet consists of five equal amplitude modes with wave numbers selected across a spectrum of undamped modes. The rms amplitude of the incoming wave packet is 0.22. The highest-frequency wave has frequency $\omega_0 =$ either 15π or 7.5π . The other modes are at $\omega_0/2$, $\omega_0/4$, $\omega_0/5$, and $\omega_0/16$. In the simulations described below, the highest frequency in the incoming wave packet is still sufficiently low so that it propagates without significant numerical damping. The cross helicity of the incoming wave modes was defined so that δv and δb were aligned (parallel or antiparallel) and the amplitudes were nearly equal, that is, $\sigma_c = -0.8$. The nonlinear time for this simulation, τ_{nl} , is approximately given by $\lambda/(2\pi[v_0 + v_A])$, where λ is wavelength of the highest-frequency mode in the wave packet. There are approximately 7 wavelengths in the box, so that $\tau_{nl} \approx 1/3$. Because it takes a time of order 1 for a wave to cross the box ($v_0/\Delta r = 1$), the wave packet is in the box for approximately $3\tau_{nl}$.

We now discuss the role of velocity shear on the cross helicity using a fairly simple set of initial conditions.

4.4. Velocity Shear

First, we describe a two-dimensional example which includes a current sheet. The plasma velocity was initialized to place the current sheet in the slow wind region and a Parker spiral field was included (but not pressure-balanced structures). The simulation was run to $t = 4$, where the unit of time is the physical time it takes a fluid element traveling at unit velocity V_r to cover a unit distance r . The simulation encompassed 120° in latitude and the slow flow occupied 40° in latitude centered at $\theta = \pi/2$.

In Plate 1 we show two-dimensional color contours of several dynamical quantities in the $r - \theta$ plane. The radial component of the velocity, $V_r(r, \theta)$, in Plate 1a shows the velocity shear separating the fast and slow flows. The values of $V_r(r, \theta)$ range from an initial low value of 1.08 in the slow flow to a high value of 2.75 the fast flow. Plate 1b shows the ϕ component of the magnetic field normalized to the WKB value so that what is plotted is $B_{\phi}(r, \theta) [\rho^{-3/4}(1 + 1/M_A)]$ [Hollweg, 1974]. The density multiplied by r^2 is plotted in Plate 1c, and $\sigma_c(r, \theta)$ is shown in Plate 1d. The simulation was run at a resolution of $600 \times 300 \times 5$. The utility of the WKB approximation for complex flows has been established by Verma and Roberts [1993], Matthaeus et al. [1994], and Zank et al. [1996].

Significant velocity gradients are evident near the boundaries between the slow and fast flows. Plate 1b illustrates by the fairly uniform intensity of the colors with r that the WKB scaling is well satisfied for these parameters. (Note the change in sign of B_ϕ across the current sheet due to the Parker spiral component which is perpendicular to the plane of the figure.) The ρr^2 contours shown in Plate 1c show an enhancement in the plasma sheet which is primarily due to the requirement of pressure balance with the magnetic field. Compressions and rarefactions in the volume are concentrated in the plasma sheet, a result of reversing the sign of the velocity fluctuations across the current sheet to preserve outward propagation. Consequently, $\nabla \cdot \mathbf{v} \neq 0$ at the current sheet [Malara et al., 1996].

The evolution of the degree of Alfvénicity of the wave packet is illustrated by the contours of $\sigma_c(r, \theta)$ shown in Plate 1d. We have “rectified” the cross helicity by multiplying by the sign of B_r so that outward propagating fluctuations have negative values of σ_c independent of the sign of B_r . Rather than smooth the fluctuations over some scale, we define σ_c to be

$$\sigma_c(r, \theta, \phi) = 2 \frac{B_\theta V_\theta}{B_\theta^2 + V_\theta^2} \left(\frac{B_r}{|B_r|} \right) \quad (9)$$

In the three-dimensional simulation, which did not include a Parker field, σ_c is defined as

$$\sigma_c(r, \theta, \phi) = 2 \frac{B_\theta V_\theta + B_\phi V_\phi}{B_\theta^2 + B_\phi^2 + V_\theta^2 + V_\phi^2} \left(\frac{B_r}{|B_r|} \right) \quad (10)$$

Because B_r reverses sign in the central current sheet, $\sigma_c = 0$ in the current sheet, initially. Once the wave packet has propagated through the domain of integration, the fluctuations in the fast flow remain Alfvénic on either side of the current sheet out to the outflow boundary at $r_{max} = 4$. The Alfvénicity remains small and chaotic in the slow flow and current sheet. There is no obvious correlation between the density and cross helicity. For example, near $r = 3 - 4$ and $\theta = \pi/2$ in the center of the plasma sheet, σ_c is rather random, but ρ is not particularly disordered.

We can examine in more detail the relationship between velocity shears, current sheets, pressure balance structures, and cross helicity by examining the results of a fully three-dimensional simulation. This simulation again spanned the radial distance from $r = 1 - 4$ and $\Delta\theta = 120^\circ$, but now $\Delta\phi = 120^\circ$. The resolution of this run was $300 \times 120 \times 120$ and included pressure-balanced flux tubes distributed in θ and ϕ , but no Parker spiral.

In Figure 3 we show plots of several quantities averaged over $r = 3 - 4$ at fixed values of ϕ . Plotted are $V_r(\theta)$ (solid line), $B_r(\theta)$ (dot-dashed line), and σ_c (dashed line). The results are similar to those shown in Figure 2 from two-dimensional simulations and from Helios observations (note that the sign convention for σ_c is opposite in the two figures). The cross helicity is large and negative, denoting outward propagating fluctuations

in the high-latitude fast wind, and variable and small in the plasma sheet and slow wind. As noted from Plate 1, the smallest values are concentrated near the center of the current sheet where the dc magnetic field rotates through 180° . These results validate the use of two-dimensional rectangular spectral method solutions of either the compressible or incompressible MHD equations in the study of solar wind turbulence, at least for the situation where the initial wave spectrum is propagating quasi-parallel to the average magnetic field. For quasi-two-dimensional initial conditions the evolution can be quite different [see Roberts et al., 1999].

The rotation of the background field introduces azimuthal magnetic fields that can be visualized by tracing magnetic field lines. In Plate 2 we show in a stereo view the source surface density at $r = 0.5$, two planes of $\mathbf{j}^2 \times r^2$ (\mathbf{j} is computed from $\nabla \times \mathbf{B}$), and several field lines. (The stereo picture must be viewed using the “cross-eyed” technique.) The current sheet appears to have reconnected magnetic field corkscrewing in the azimuthal direction. The topology of the field suggests that there has been significant reconnection. Whereas most of the field lines at high and low latitudes generally lie parallel to the radial direction, many which connect to the outflow boundary close to the current sheet meander considerably, reconnect in the central current sheet, and leave the flux rope region in another direction. In the inner region ($r < 2$), there are large loops of magnetic flux which are connected to the source surface.

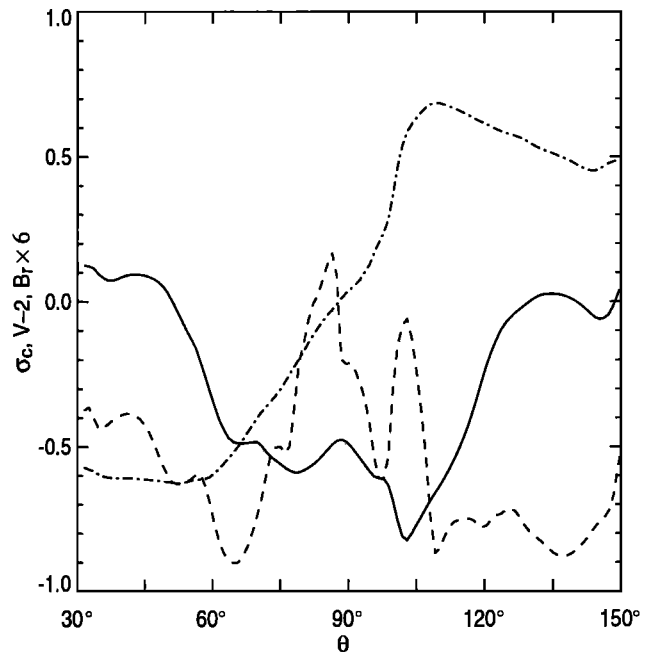


Figure 3. Velocity shear and cross helicity from the three-dimensional spherical expansion code. The current sheet is indicated by the change in sign of B_r (dot-dashed line); the velocity shear by V_r (solid line), and the normalized cross helicity σ_c (dashed line). The values have been averaged over the interval $r = 3 - 4$.

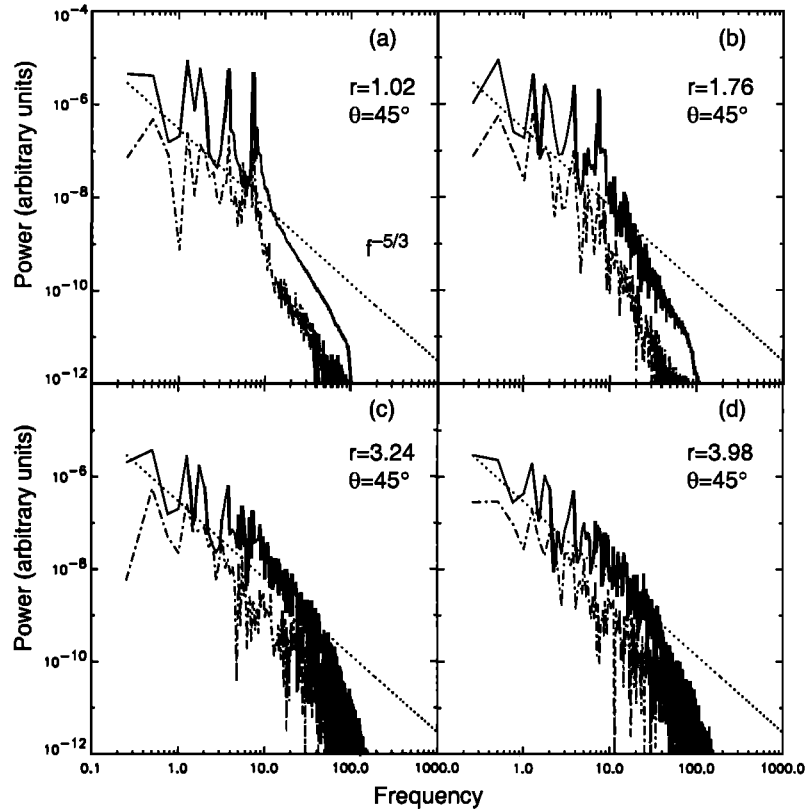


Figure 4. Trace of the power spectral matrix of the reduced power spectrum of the time series of the magnetic field components and $|B|$ (dashed line) along a radius in the high speed flow at $\theta = 45^\circ$: (a) $r = 1.02$; (b) $r = 1.76$; (c) $r = 3.24$; and (d) $r = 3.98$. Also shown on each plot is a line with slope $5/3$.

One must be cautious, however, about attributing physical significance to this particular simulation for the actual solar wind and heliospheric current sheet. All of the reconnection results from numerical resistivity, which, for the relatively low resolution of this solution, is very much greater than that in the solar wind. Nonetheless, it is intriguing to see how field lines near the current sheet can reconnect in three dimensions. The resulting structures are reminiscent of “magnetic clouds” and may prove useful for studying the dynamics of such objects.

4.5. Power Spectra

Of particular interest is to see if an Alfvénic wave packet comprising only five modes can evolve to a turbulent state in a spherically expanding domain. From data collected from the two-dimensional simulations at particular points and every time step, and in direct analogy to how spectra are calculated from single spacecraft observations, we constructed time series of the magnetic and velocity fields and density. The numerical data were obtained by placing 20 “probes” in the r, θ plane. The time series were detrended and then Fourier transformed [cf., e.g., *Matthaeus and Goldstein, 1982*].

In Figure 4 we show sample power spectra in the high speed flow at $\theta = 45^\circ$. Four spectra are plotted at

$r = 1.02$ near the inflow boundary, at $r = 1.76$ about $1/4$ of the way out from r_0 , at $r = 3.24$ about $3/4$ of the way out from r_0 , and near the outflow boundary at $r = 3.98$. At $r = 1.02$ the five modes constituting the initial wave packet are dominant, but even at this location some evolution is evident because the power levels of the five modes are no longer equal. By $r = 3.24$, the spectrum has evolved to the point where the initial wave modes are less pronounced. The spectrum near the outflow boundary suggests that the fluid has undergone significant evolution—at least to the extent that the level of the initial wave packet now approximates a spectrum with a power law slope of $\sim f^{-5/3}$. It is less clear from these results whether a true cascade to frequencies higher than those input initially has occurred. While there are certainly high frequencies present in the spectra shown in Figure 4, the slope of the high frequency portion of the spectrum is close to $\sim f^{-2}$, reflecting the fact that the compressive interactions, especially near the central current sheet, have steepened into shock waves. This may be a consequence of having chosen a rather small value of $\beta = 0.25$, which enhances “decay-like” interactions and leads to excitation of sound waves [*Wong and Goldstein, 1986*].

Besides the fact that the spectra appear to be evolving toward a Kolmogoroff-like state, there is signifi-

cantly less power in fluctuations in $|B|$ (dot-dashed line) than there is in the trace of the spectral tensor (solid line). The relatively small amount of power in $|B|$ is also a common feature of interplanetary spectra. Because of the relatively fast flow, the time available for a cascade of energy to small scales is limited. The frequency range of the initial packet was chosen to allow room in spectral space for a cascade to appear without significant numerical dissipation. Nonetheless, it is difficult to determine from these spectra the extent to which a cascade is being slowed or inhibited by the spherical expansion and its attendant increase in spatial scales.

For comparison, in Figure 5 we show spectra constructed from a single radial line in the slow speed flow. The radial distances of the four spectra are the same as in Figure 4. In general the spectra computed from fluctuations in the slow flow are similar to those computed from the fast flow except that at relatively small r the spectrum is more evolved and by $r = 3.98$, the spectrum has evolved to a rather featureless power law. The approximate power law extends to higher frequencies in the slow flow than it did in the fast flow.

4.6. Pressure-Balanced Flux Tubes

We now turn to a more detailed discussion of the fully three-dimensional simulations which included pressure-balanced flux tubes in addition to the current sheet.

In Plate 3 (top) we show the initial density contours (bright small image) at the inflow boundary ($r_0 = 1.0$) from the three-dimensional run which included pressure-balanced flux tubes distributed in θ and ϕ . The variations of density with ϕ reflect the pressure-balanced flux tubes. No Parker spiral field was included.

The flux tubes have a significant effect on the evolution of the Alfvénic wave packet. The transparent surface, located at $r \sim 4$, is σ_c . The high Alfvénicity of the original wave packet has changed substantially due to the current sheet, the velocity shear layers, and the flux tubes. The asymmetry between the northern and southern hemispheres arises from the staggered distribution in θ of the flux tubes that results when the wave number $k_\theta = 2$ in (7).

4.7. Spectral Anisotropies

From both incompressible and compressible spectral method simulations in two and three dimensions and analytic work, we know that a strong dc component of the magnetic field influences the rate at which nonlinear mode couplings occur in directions parallel and transverse to the direction of the average magnetic field. The tendency of magnetic fluctuations to become highly anisotropic when a strong magnetic field is present has been confirmed in a series of simulations [Shebalin et al., 1983; Goldstein et al., 1987, 1989; Roberts et al., 1992; Matthaeus and Lamkin, 1985; Matthaeus et al.,

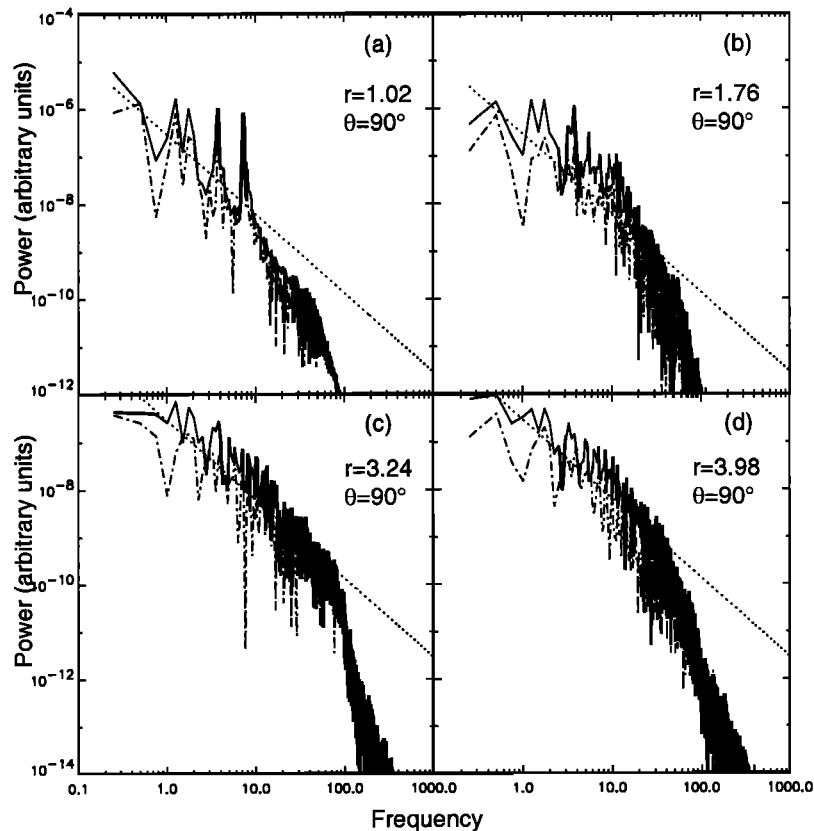


Figure 5. Same as Figure 6, but along a radial line in the slow speed flow at $\theta = 90^\circ$ colatitude.

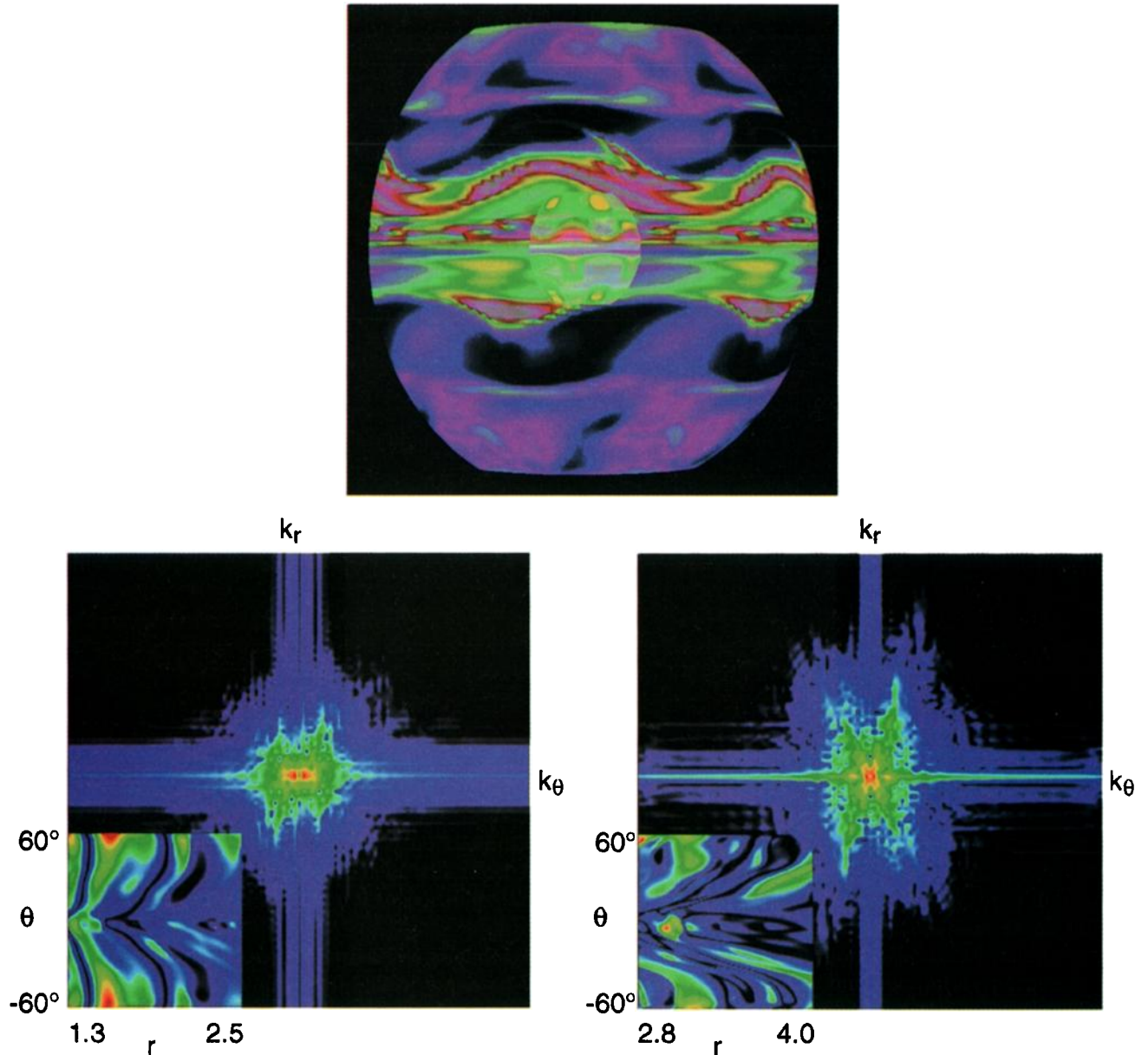


Plate 3. (top) Two color surfaces from the three-dimensional simulation. The bright opaque surface is density at $r_0 = 1.0$. A transparent surface of σ_c is at located at $r \sim 4$ and shows the influence on the Alfvénicity of the current sheet, velocity shear layers, and flux tubes. (bottom) Two-dimensional power spectra of $B_\theta(k_r, k_\theta)$ at two radial positions. The spectra are taken at $\phi = 26^\circ$ in the $r - \theta$ plane. The spectrum on the left covers the region near the inflow and the one on the right covers a region closer to the outflow. The insets are the configuration space contours of $B_\theta(r, \phi)$

1996; Oughton *et al.*, 1994, 1998; Ghosh and Goldstein, 1997; Ghosh *et al.*, 1998a,b]. There is no theoretical prediction, however, as to how a dc field will affect the development of the magnetic spectral tensor in expanding geometries.

Using a three-dimensional compressible pseudospectral algorithm, Ghosh *et al.* [1993, 1998a] explored the development of spectral cascades in Cartesian geometry. Initially, the cubic domain of integration was filled with both pressure-balanced structures and with field-

aligned Alfvénic fluctuations which they referred to as slab modes. This initial condition produced a turbulent cascade unlike that seen in earlier studies [Shebalin *et al.*, 1983; Matthaeus *et al.*, 1996], all of which began with isotropic initial conditions. Ghosh *et al.* [1998a] found that after a few nonlinear times, the spectrum became highly oblique, but not purely perpendicular, mainly due to the refraction of the waves by the inhomogeneities transverse to the flow. This contrasted with the results using isotropic initial conditions for

which the anisotropies did evolve to a pure perpendicular alignment. A comparison of those results with the state of the fluid near the end of the box as shown in Plate 3 (bottom) shows that the expanding geometry produces the same spectral evolution in that there is a strong refraction effect but also a deficit in power in purely k_{\perp} modes. The configuration space plot of B_{θ} also suggests the presence of reconnection near the current sheet. We shall explore this phenomenon further in a subsequent publication.

5. Discussion

Previous simulations using the MHD equations to study solar wind turbulence were confined to Cartesian geometry. Those results indicated that the evolution of Alfvénic fluctuations in the solar wind is driven primarily by velocity shears or proximity to the heliospheric current sheet where the interplanetary magnetic field reverses sign. The solutions presented here generalize those studies to three-dimensional spherically expanding flows. One motivation for this study was to ascertain the role played by expansion in modulating turbulent evolution. For several years there has been a debate as to whether or not the expansion of the solar wind would reduce the nonlinear interactions as the length scales and interaction times increased with radial distance [see, e.g., *Grappin et al.*, 1993a,b; *Grappin and Velli*, 1996]. The model developed by Grappin et al. solved the MHD equations in comoving coordinates that expanded as time progressed. On the basis of this expanding box model, Grappin [1995] concluded that “the spectral formation is stopped by the expansion, while an already developed spectrum suffers self-similar decay, and ... the spectral formation itself is strongly hindered by the expansion.” One important difference between the initial conditions used by Grappin [1995] and Grappin and Velli [1996] and those used here is that their velocity shear layer was very mild. In addition, the flat initial spectrum of modes that we used in our initial conditions is more likely to drive a turbulent cascade than is the single mode they used. Although the results presented here do suggest that the nonlinear interactions leading to a cascade are operating and are driving the spectrum toward a $k^{-5/3}$ shape, the simulation domain was probably not long enough for a definitive result to emerge. Further results of our study of spectral evolution in spherical geometries together with a comparison to evolution in Cartesian geometry will be reported elsewhere.

Our solutions suggest that at least for parallel propagating Alfvén waves, spectral evolution proceeds in much the same manner as in Cartesian geometry, albeit more slowly. For the physical parameters used, this corresponds to a radial distance in the solar wind from approximately 20–40 R_S . Radial expansion does, however, have a profound effect on the evolution of some classes of fluctuations. For example, Roberts et

al. [1999] showed that the evolution of two-dimensional fluctuations was slowed significantly by expansion.

Leaving aside the question of how two-dimensional turbulence is affected by expansion, it is clear from the results presented above that, as in Cartesian geometry, the cross helicity of an Alfvénic wave packet evolves rapidly in the vicinity of strong velocity shears. When pressure-balanced structures are also present, the compressible interactions introduced also diminish σ_c . The importance of compressibility is most evident in the current sheet where, because of the change in sign of the radial magnetic field and the necessity to change the sign of the velocity fluctuations to ensure outward propagation, waves are refracted into the current sheet and $\nabla \cdot \mathbf{v} \neq 0$, resulting in large fluctuations in the density.

6. Conclusions

We have presented results from a new three-dimensional solution of the MHD equations in spherical geometry. These simulations were designed to investigate the extent to which spherical expansion affects the development of turbulence. The FCT algorithm we used has minimal numerical dissipation, preserves $\nabla \cdot \mathbf{B} = 0$ to machine round-off, and allows for quite general initial and boundary conditions. Our results support the theoretical studies [Hollweg, 1974; Verma and Roberts, 1993; Matthaeus et al., 1994; Zank et al., 1996] that predicted that $\delta \mathbf{B}_{\perp}$ and $\delta \mathbf{V}_{\perp}$ satisfy the WKB approximation over the radial range covered in our simulations. A major focus of this study has been to investigate the role of velocity shears and current sheets on the evolution of Alfvénic fluctuations. In addition, the algorithm has sufficient generality to include a Parker spiral field and co-rotating interaction regions. We have shown that with only velocity shear layers and a current sheet, initially nearly pure Alfvénic wave packets ($\sigma_c = -0.8$) will lose their Alfvénicity in the vicinity of the velocity shears and the current sheet, resulting in small or positive values of σ_c . When pressure-balanced structures are added to the flow, they too lead to a decrease in σ_c , but less effectively than the velocity shears and current sheet.

We also accumulated time series of the dynamical variables from which reduced power spectra can be computed. We constructed power spectra of \mathbf{B} , \mathbf{V} , and ρ in fast or slow wind, near or far from the current sheet. Even with the modest resolution of the present simulations, the sample spectra in Figures 4 and 5 show that there is a tendency for power-law power spectrum to form. The spectral index approaches $5/3$ at late times and large distances.

The two-dimensional spectra we computed are similar to those obtained previously in Cartesian geometry [Shebalin et al., 1983; Matthaeus et al., 1996; Ghosh et al., 1998a] in that there is a tendency for the spectra to be anisotropic. This tendency is probably enhanced by the expansion since the transverse scale lengths are

increasing with radius more rapidly than are the radial scale lengths. Further studies of the evolution of two-dimensional turbulence and the relationship between anisotropic spectra and the “Maltese Cross” correlation function will be deferred to subsequent work. Although our results for Alfvénic fluctuations show that turbulent spectra will arise in some circumstances despite the expansion [cf. Grappin and Velli, 1996], Roberts *et al.* [1999] have reported that the evolution of pure two-dimensional turbulence is slowed dramatically in spherical coordinates. Furthermore, it is as yet unclear whether a true cascade of energy to scales smaller than those of the input wave packet occurs.

Future studies will generalize the initial and boundary conditions and will include interaction regions. In addition, at higher resolution, we will be able to investigate magnetic reconnection and its role in determining the geometry of the solar wind magnetic fields in the current sheet.

Acknowledgments. The authors would like to thank the referees for their helpful suggestions which increased the accuracy and clarity of the presentation. MLG would like to thank L. Ofman, D. Burgess, and S. Schwartz for many stimulating discussions. This research was supported by NASA’s Space Physics Theory Program in “The Role of Turbulence in Heliospheric Plasmas” at the Goddard Space Flight Center. AED acknowledges support from NASA grant NAG-56152 to the University of Maryland, College Park.

Janet G. Luhmann thanks Francesco Malara and Roberto Bruno for their assistance in evaluating this paper.

References

- Bavassano, B., and R. Bruno, Evidence of local generation of Alfvénic turbulence in the solar wind, *J. Geophys. Res.*, **94**, 11,977, 1989.
- Bavassano, B., E. Pietropaolo, and R. Bruno, Cross-helicity and residual energy in solar wind turbulence: Radial evolution and latitudinal dependence in the region from 1 to 5 AU, *J. Geophys. Res.*, **103**, 6521, 1998.
- Belcher, J.W., and L. Davis, Large-amplitude Alfvén waves in the interplanetary medium, *J. Geophys. Res.*, **76**, 3534, 1971.
- Bieber, J., W.H. Matthaeus, C.W. Smith, M.-B. Kallenrode, and G. Wibberenz, Proton and electron mean free paths: The Palmer consensus revisited, *Astrophys. J.*, **420**, 294, 1994.
- Boris, J. P., D.L. Book, Flux corrected transport I: SHASTA A fluid transport algorithm that works, *J. Comput. Phys.*, **11**, 38, 1973.
- Bruno, R., and B. Bavassano, Origin of low cross-helicity regions in the inner solar wind, *J. Geophys. Res.*, **96**, 7841, 1991.
- Bruno, R., B. Bavassano, and U. Villante, Evidence for long period Alfvén waves in the inner solar system, *J. Geophys. Res.*, **90**, 4373, 1985.
- Burlaga, L.F., and K.W. Ogilvie, Magnetic and thermal pressures in the solar wind, *Sol. Phys.*, **15**, 61, 1970.
- Carbone, V., F. Malara, and P. Veltri, A model for the three-dimensional magnetic field correlation spectra of low-frequency solar wind fluctuations during Alfvénic periods, *J. Geophys. Res.*, **100**, 1763, 1995.
- Coleman, P.J., Wave-like phenomena in the interplanetary plasma: Mariner 2, *Planet. Space Sci.*, **15**, 953, 1967.
- Coleman, P.J., Turbulence, viscosity, and dissipation in the solar wind plasma, *Astrophys. J.*, **153**, 371, 1968.
- Deane, A., *solwind*: A 3D compressible MHD code for Solar Wind studies. version 1.0: Cartesian coordinates, *Tech. Rep. CR 4725*, NASA Goddard Space Flight Cent., Greenbelt, Md., 1996.
- DeVore, C.R., Flux-corrected transport techniques for multidimensional compressible magnetohydrodynamics, *J. Comput. Phys.*, **92**, 142, 1991.
- Elsässer, W. M., The hydromagnetic equations, *Phys. Rev.*, **79**, 183, 1950.
- Elsässer, W. M., Hydromagnetic dynamo theory, *Rev. Mod. Phys.*, **18**, 135, 1956.
- Ghosh, S., and M.L. Goldstein, Anisotropy in Hall MHD turbulence due to a mean magnetic field, *J. Plasma Phys.*, **57**, 129, 1997.
- Ghosh, S., M. Hossain, and W.H. Matthaeus, The application of spectral methods in simulating compressible fluid and magnetofluid turbulence, *Comput. Phys. Commun.*, **74**, 18, 1993.
- Ghosh, S., W.H. Matthaeus, D.A. Roberts, and M.L. Goldstein, The evolution of slab turbulence in the presence of pressure balanced structures and velocity shears, *J. Geophys. Res.*, **103**, 23,691, 1998a.
- Ghosh, S., W.H. Matthaeus, D.A. Roberts, and M.L. Goldstein, Waves, structures, and the appearance of two-component turbulence in the solar wind, *J. Geophys. Res.*, **103**, 23,705, 1998b.
- Goldstein, M.L., D.A. Roberts, and A. Deane, Numerical simulation of MHD turbulence in three dimensions, in *Correlated phenomena at the Sun, in the Heliosphere and in Geospace*, edited by A. Wilson, *Eur. Space Agency Spec. Publ.*, **SP-415**, 83, 1997.
- Goldstein, M.L., D.A. Roberts, S. Ghosh, and W.H. Matthaeus, Numerical simulation of solar wind and magnetospheric phenomena, in *21st ESLAB Symposium*, edited by B. Battrock and E.J. Rolfe, **115**, Eur. Space Agency, Bolkesjø, Norway, 1987.
- Goldstein, M.L., D.A. Roberts, and W.H. Matthaeus, Numerical simulation of interplanetary and magnetospheric phenomena: The Kelvin-Helmholtz instability, in *Solar System Plasma Physics, Geophys. Monogr. Ser.*, vol. 54, edited by J.H. Waite, Jr., J.L. Burch, and R.L. Moore, p. 113, AGU, Washington, D. C., 1989.
- Goldstein, M.L., D.A. Roberts, and W.H. Matthaeus, Magnetohydrodynamic turbulence in the solar wind, *Ann. Rev. Astron. Astrophys.*, **33**, 283, 1995.
- Goldstein, M.L., D.A. Roberts, and W.H. Matthaeus, Magnetohydrodynamic turbulence in cosmic winds, in *Cosmic Winds and the Heliosphere*, edited by J.R. Jokipii, C.P. Sonett, and M.S. Giampapa, p. 521, Univ. of Ariz. Press, Tucson, 1997.
- Grappin, R., Onset of anisotropy and Alfvén wave turbulence in the expanding solar wind, in *Eighth International Solar Wind Conference*, edited by D. Winterhalter *et al.*, p. 306, AIP Press, College Park, Md., 1995.
- Grappin, R., A. Mangeney, and E. Marsch, On the origin of solar wind MHD turbulence: Helios data revisited, *J. Geophys. Res.*, **95**, 8197, 1990.
- Grappin, R., and M. Velli, Waves and streams in the expanding solar wind, *J. Geophys. Res.*, **101**, 425, 1996.
- Grappin, R., M. Velli, and A. Mangeney, “Alfvénic” versus “standard” turbulence in the solar wind, *Ann. Geophys.*, **9**, 416, 1991.
- Grappin, R., M. Velli, and A. Mangeney, MHD simulations of solar wind turbulence in comobile coordinates, in *Spatio-Temporal Analysis for Resolving Plasma Turbulence (START)*, p. 325, Eur. Space Agency, Aussois, France, 1993a.

- Grappin, R., M. Velli, and A. Mangeney, Nonlinear wave evolution in the expanding solar wind, *Phys. Rev. Lett.*, **70**, 2190, 1993b.
- Hollweg, J.V., Transverse Alfvén waves in the solar wind: Arbitrary \mathbf{k} , \mathbf{v}_0 , \mathbf{B}_0 , and $|\delta\mathbf{B}|$, *J. Geophys. Res.*, **79**, 1539, 1974.
- Malara, F., L. Primavera, and P. Veltri, Compressive fluctuations generated by time evolution of Alfvénic perturbations in the solar wind current sheet, *J. Geophys. Res.*, **101**, 21,597, 1996.
- Malara, F., P. Veltri, and L. Primavera, Nature of the density-magnetic-field-intensity correlation observed in solar wind, *Phys. Rev. E*, **56**, 3508, 1997.
- Marsch, E., and C.-Y. Tu, Dynamics of correlation functions with Elsässer variables for inhomogeneous MHD turbulence, *J. Plasma Phys.*, **41**, 479, 1989.
- Marsch, E., and C.-Y. Tu, On the radial evolution of MHD turbulence in the inner heliosphere, *J. Geophys. Res.*, **95**, 8211, 1990a.
- Marsch, E., and C.-Y. Tu, Spectral and spatial evolution of compressive turbulence in the inner solar wind, *J. Geophys. Res.*, **95**, 11, 1990b.
- Matthaeus, W.H., and M.L. Goldstein, Measurement of the rugged invariants of magnetohydrodynamic turbulence, *J. Geophys. Res.*, **87**, 6011, 1982.
- Matthaeus, W.H., and S.L. Lamkin, Rapid magnetic reconnection caused by finite amplitude fluctuations, *Phys. Fluids*, **28**, 303, 1985.
- Matthaeus, W.H., M.L. Goldstein, and D.A. Roberts, Evidence for the presence of quasi-two-dimensional, nearly incompressible fluctuations in the solar wind, *J. Geophys. Res.*, **95**, 20,673, 1990.
- Matthaeus, W.H., L.W. Klein, S. Ghosh, and M.R. Brown, Nearly incompressible magnetohydrodynamics, pseudosound, and solar wind fluctuations, *J. Geophys. Res.*, **96**, 5421, 1991.
- Matthaeus, W.H., Y. Zhou, G.P. Zank, and S. Oughton, Transport theory and the WKB approximation for interplanetary MHD fluctuations, *J. Geophys. Res.*, **99**, 23,421, 1994.
- Matthaeus, W.H., S. Ghosh, S. Oughton, and D.A. Roberts, Anisotropic three-dimensional MHD turbulence, *J. Geophys. Res.*, **101**, 7619, 1996.
- Montgomery, D., M. Brown, and W.H. Matthaeus, Density fluctuation spectra in magnetohydrodynamic turbulence, *J. Geophys. Res.*, **92**, 282, 1987.
- Oughton, S., E. Priest, and W.H. Matthaeus, The influence of a mean magnetic field on three dimensional MHD turbulence, *J. Fluid Mech.*, **280**, 95, 1994.
- Oughton, S., W.H. Matthaeus, and S. Ghosh, Scaling of spectral anisotropy with magnetic field strength in decaying MHD turbulence, *J. Plasma Phys.*, **5**, 4235, 1998.
- Parker, E.N., *Interplanetary Dynamical Processes*, Wiley Intersci., New York, 1963.
- Parker, E.N., Dynamical properties of solar and stellar winds, III, *Astrophys. J.*, **139**, 690, 1964.
- Roberts, D.A., Heliocentric distance and temporal dependence of the interplanetary density-magnetic field magnitude correlation, *J. Geophys. Res.*, **95**, 1087, 1990.
- Roberts, D.A., M.L. Goldstein, L.W. Klein, and W.H. Matthaeus, Origin and evolution of fluctuations in the solar wind: Helios observations and Helios-Voyager comparisons, *J. Geophys. Res.*, **92**, 12,023, 1987a.
- Roberts, D.A., M.L. Goldstein, L.W. Klein, and W.H. Matthaeus, The nature and evolution of magnetohydrodynamic fluctuations in the solar wind: Voyager observations, *J. Geophys. Res.*, **92**, 11,021, 1987b.
- Roberts, D.A., S. Ghosh, M.L. Goldstein, and W.H. Matthaeus, MHD simulation of the radial evolution and stream structure of solar wind turbulence, *Phys. Rev. Lett.*, **67**, 3741, 1991.
- Roberts, D.A., M.L. Goldstein, W.H. Matthaeus, and S. Ghosh, Velocity shear generation of solar wind turbulence, *J. Geophys. Res.*, **97**, 17,115, 1992.
- Roberts, D.A., M.L. Goldstein, and A. Deane, Quasi-two-dimensional MHD turbulence in three-dimensional flows, *Phys. Rev. Lett.*, **85**, 548, 1999.
- Sari, J.W. and G.C. Valley, Interplanetary magnetic field power spectra: Mean field radial or perpendicular to radial, *J. Geophys. Res.*, **81**, 5489, 1976.
- Shebalin, J.V., W.H. Matthaeus, and D. Montgomery, Anisotropy in MHD turbulence due to a mean magnetic field, *J. Plasma Phys.*, **29**, 525, 1983.
- Stribling, T., D.A. Roberts, and M.L. Goldstein, A three-dimensional magnetohydrodynamic model of the inner heliosphere, *J. Geophys. Res.*, **101**, 27,603, 1996.
- Taylor, G.I., The spectrum of turbulence, *Proc. R. Soc. London, Ser. A*, **164**, 476, 1938.
- Vellante, M., and A.J. Lazarus, An analysis of solar wind fluctuations between 1 and 10 AU, *J. Geophys. Res.*, **92**, 9893, 1987.
- Verma, M., and D.A. Roberts, The radial evolution of the amplitudes of "dissipationless" turbulent solar wind fluctuations, *J. Geophys. Res.*, **98**, 5625, 1993.
- Wong, H. K., and M. L. Goldstein, Parametric instabilities of circularly polarized Alfvén waves including dispersion, *J. Geophys. Res.*, **91**, 5617, 1986.
- Zalesak, S.T., Fully multidimensional flux-corrected transport algorithms for fluids, *J. Comput. Phys.*, **31**, 335, 1979.
- Zank, G.P., W.H. Matthaeus, and C.W. Smith, Evolution of turbulent magnetic fluctuation power with heliospheric distance, *J. Geophys. Res.*, **101**, 17,093, 1996.

A. E. Deane, Institute for Physical Science and Technology University of Maryland, College Park, MD 20742

M. L. Goldstein, D. A. Roberts, S. Ghosh, and H. K. Wong, Code 692, NASA Goddard Space Flight Center, Greenbelt, MD 20771.

(Received May 7, 1998; revised November 19, 1998; accepted November 19, 1998.)